

Simulations of transiently heated solar coronal loops

D. Spadaro and A.F. Lanza

INAF, Osservatorio Astrofisico di Catania, via S. Sofia 78, 95123 Catania, Italy
e-mail: dsp@ct.astro.it

Abstract. This is a short summary of a paper recently published in The Astrophysical Journal. We investigate the hydrodynamic behaviour of coronal loops undergoing transient heating. We adopt a 1-D loop model with space- and time-dependent heating, concentrated near the chromospheric footpoints. The timescale of heating variations is comparable with the radiative cooling time of the coronal plasma ($\sim 10^3$ s). We describe the temporal behaviour of the various physical quantities (plasma density, temperature, flow velocity) along some modelled loops with different heating terms.

Key words. Solar corona – Transition region – Coronal heating

1. Introduction

We investigate the hydrodynamic behaviour of coronal loops undergoing transient heating. This work has been stimulated by the recent observations of the solar transition region and corona with the EUV spectrometers and imagers on board the space missions SOHO and TRACE, which show evidence for significant plasma flows and intensity variations in non-flaring magnetic loops.

We adopt a 1-D loop model with space- and time-dependent heating, concentrated near the chromospheric footpoints, and simulate the hydrodynamics of loops with different effective gravity (i.e., different loop geometry) and heating terms. The

timescale of heating variations is comparable with the radiative cooling time of the coronal plasma ($\sim 10^3$ s). We use a numerical code that has a fully adaptive grid, in order to properly resolve the chromospheric-coronal transition region sections of the loop.

We present in this paper the results concerning some simulated loops, referring the reader to Spadaro et al. (2003) for a complete description of the investigation.

2. 1-D loop model

We adopt a loop model symmetric about its midpoint (top), not necessarily semi-circular, whose geometry is described by the loop total length, L , and the loop apex height, h . The height above the chromospheric footpoints as a function of the curvilinear coordinate along the field lines

Send offprint requests to: D. Spadaro
Correspondence to: Via S. Sofia 78, 95123 Catania

s , $z(s)$, is equal to 0 at the footpoints and has its maximum h at the midpoint; moreover, $dz/ds = \pm 1$ at the footpoints (Spadaro et al. 2003).

The simulations reported here have a length of the coronal portion of the loop approximately equal to 80,000 km and a height at the top of 14,000 km. In addition, the numerical model includes a deep chromosphere (60,000 km at a temperature $\sim 3 \times 10^4$ K) at each footpoint, so that the total length of the loop is 200,000 km (see also Karpen et al. 2001).

We solve the basic equations describing the behaviour of the fully ionized hydrogen loop plasma, i.e., the mass continuity, the momentum equation and the energy equation as described in Spadaro et al. (2003). The heating term, $E(s, t)$, appearing in the energy equation is given by a constant uniform background heating E_0 , plus a transient spatially localized heating $E_1(s, t)$, so that:

$$\begin{aligned} E(s, t) &= E_0 + E_1(s, t) \quad (\text{erg cm}^{-3} \text{ s}^{-1}) \\ E_1(s, t) &= qf\gamma(t) \exp[-(s - s_1)/\lambda] \\ \gamma(t) &= \begin{cases} \sin \frac{\pi(t-t_0)}{3000} & t_0 \leq t \leq t_0 + 3000 \text{ s} \\ 0 & \text{elsewhere} \end{cases} \end{aligned} \quad (1)$$

where s_1 is the location of the top of the chromosphere, $\lambda = 10^9$ cm, q the maximum transient heating rate (in $\text{erg cm}^{-3} \text{ s}^{-1}$), f the ratio of the localized heating at the right to that at the left footpoint and t_0 the time when the transient heating starts.

Antiochos et al. (1999, 2000) describe in detail ARGOS, the code adopted to solve the plasma equations. It makes use of a fully adaptive grid implemented by means of the parallel adaptive mesh refinement package (PARAMESH, MacNeice et al. 2000).

We refer the reader to Spadaro et al. (2003), for an ample discussion about the boundary conditions imposed at the two endpoints, as well as the treatment of the chromospheric radiative losses. We have calculated three loop models, varying the values of the parameters introduced above. These values are listed in Table 1.

Table 1. *Parameters of the simulated loops.*

Loop	q ($\text{erg cm}^{-3} \text{ s}^{-1}$)	f
1	1.0×10^{-2}	0.75
2	1.0×10^{-1}	0.75
3	1.0×10^{-2}	0.25

Note: $L/2 = 4 \times 10^9$ cm, $h = 1.4 \times 10^9$ cm and $E_0 = 3.8 \times 10^{-5}$ $\text{erg cm}^{-3} \text{ s}^{-1}$ in all the loops.

3. Results

To derive the initial equilibrium of the loop, we let the system evolve as described in Antiochos et al. (1999, 2000).

After $\sim 20,000$ s the loop settles into a static equilibrium with negligible residual motions. We take this state as the initial equilibrium, $t = 0$ s. Figures 1-3 show the temperature, density, and velocity as functions of distance along the loop at this time (solid lines).

We then turn on the spatially and temporally dependent heating, E_1 , according to Equations 1. Figures 1-3 also report the temperature, density and velocity profiles along the loops at other selected times during their evolution.

The temporal behaviour of the various physical quantities along the loops shows that the increase in heating (lasting 3,000 s) produces a chromospheric evaporation in both the legs, with maximum flow velocities corresponding to the highest amount of localized heating ($t \sim 1,500$ s, dotted lines), and an increase of the plasma density and temperature at the top of the loop. Increasing the transient heating rate q , for $f = 0.75$ (loops 1 and 2), we note an increase in the quantity of evaporating chromospheric material and in the evaporation velocity (from a few to 20-30 km s^{-1}). However, the density is still increasing at the time of temperature maximum because the model loop has not yet reached equilibrium (see, e.g., Figure 2). Hence the loop

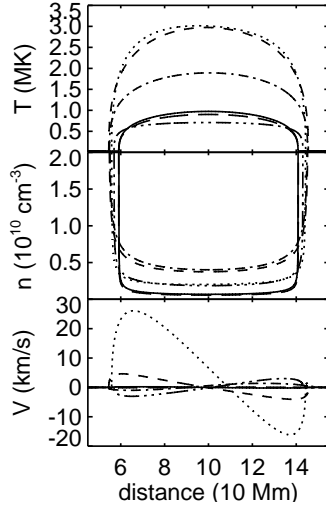


Fig. 1. Temperature T , electronic density n_e and velocity V vs. the distance along the loop from the left footpoint for Loop 1. Different times are indicated with different line styles, i.e.: initial condition ($t = 0$) – solid line; near the maximum heating rate ($t = 1504$ s) – dotted; near the end of the transient heating ($t = 2978$ s) – dashed; beginning of the downflow ($t = 5970$ s) – dashed dot; maximum of the downflow ($t = 14958$ s) – dash dot dot dot; restored initial condition ($t = 27913$ s) – long dashed.

would appear to be hot and underdense, assuming a filling factor of unity.

Due to the heating asymmetry with respect to the loop midpoint, the temperature and flow velocity are slightly higher in the left leg than in the right leg. In the case of loop 3 (Figure 3), where the heating asymmetry between the loop footpoints is stronger ($f = 0.25$), we note a net siphon flow from left to right soon after the beginning of the localized heating (maximum siphon flow velocity of about 50 km s^{-1} at $t = 670$ s), followed by an evaporation with a certain degree of asymmetry in both legs similar to that noticed in the other loop models.

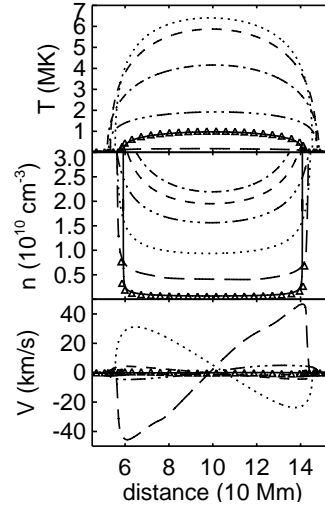


Fig. 2. As in Fig. 1, for Loop 2. Different times are indicated with different line styles, i.e.: initial condition ($t = 0$) – solid line; near the maximum heating rate ($t = 1503$ s) – dotted; near the end of the transient heating ($t = 2999$ s) – dashed; beginning of the downflow ($t = 5033$ s) – dashed dot; significant downflow ($t = 10000$ s) – dash dot dot dot; immediately before the catastrophic cooling ($t = 14172$ s) – long dashed; restored initial condition ($t = 31875$ s) – open triangles.

When the localized heating ends, the loop plasma begins to cool and drain toward the chromospheric footpoints. This long-lasting phase (about 5-6 times the period of localized heating) is characterized by downflows in both the legs, and by a progressive decrease of the density and temperature at the top of the loop. We note, however, a time lag between the heating turnoff and the draining phase: the density continues to rise as the temperature starts to decrease and, in fact, overshoots the equilibrium value predicted for a static loop with the same coronal temperature (see, e.g., Figure 2).

The downflow velocity increases as the

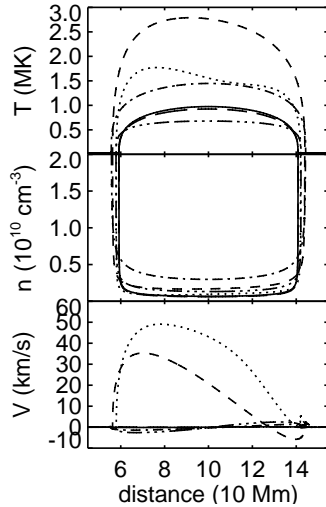


Fig. 3. As in Fig. 1, for Loop 3. Different times are indicated with different line styles, i.e.: initial condition ($t = 0$) – solid line; maximum siphon flow ($t = 670$ s) – dotted; near maximum transient heating ($t = 1544$ s) – dashed; beginning of the downflow ($t = 7641$ s) – dashed dot; near maximum of the downflow ($t = 16641$ s) – dash dot dot dot; restored initial condition ($t = 28278$ s) – long dashed.

heating rate q increases (see Table 1), but is of some km s^{-1} at most, except in loop 2 (characterized by $q = 10^{-1} \text{ erg cm}^{-3} \text{ s}^{-1}$), where a catastrophic cooling with high downflows ($\sim 50\text{--}80 \text{ km s}^{-1}$) appears approximately 11,000 after the end of the transient heating phase (long dashed lines in Figure 2).

About 20,000–30,000 s after the end of the localized heating, the loops settle again into a state with negligible motions (long dashed lines in Figures 1 and 3, open triangles in Figure 2), nearly identical to the initial static equilibrium before the spatially dependent heating turn on. Some features

of our results may have important implications for our understanding of the observed properties of coronal loops. We propose, for instance, that the evolutionary sequence described above explains both the apparent underdensity of most hot Yohkoh loops (Porter & Klimchuk 1995) and the overdense loops observed by TRACE and SOHO (Aschwanden et al. 1999, 2000).

Furthermore, strong transient heating can account for the catastrophic loop cooling and evacuation reported by Schrijver (2001). We note that loop 2 (see Figure 2) greatly undershoots its initial temperature and cools down to values well below 10^5 K, while downflows up to 80 km s^{-1} effectively empty a large fraction of the enhanced coronal mass onto the chromosphere. We refer the reader to Spadaro et al. (2003) for a wider discussion of the hydrodynamic simulations reported here and of those relevant to other loops with different lengths and shapes. Spadaro et al. also estimate the EUV plasma emission predicted by the loop models, for comparison with SOHO and TRACE observations.

References

- Antiochos, S.K., MacNeice, P.J., Spicer, D.S. & Klimchuk, J.A. 1999, *ApJ* 512, 985
- Antiochos, S.K., MacNeice, P.J. & Spicer, D.S. 2000, *ApJ* 536, 494
- Aschwanden, M.J., Newmark, J.S., Delaboudinière, J.-P. et al. 1999, *ApJ* 515, 842
- Aschwanden, M.J., Alexander, D., Hurlburt, N. et al. 2000, *ApJ* 531, 1129
- Karpen, J.T., et al. 2001, *ApJ* 553, L85
- MacNeice, P.J., et al. 2000, *Comput. Phys. Commun.* 126, 330
- Porter, L.J. & Klimchuk, J.A. 1995, *ApJ* 454, 499
- Schrijver, C.J. 2001, *Sol. Phys.* 198, 325
- Spadaro, D., et al. 2003, *ApJ* 582, 486